

Supporting Information

Surface-Confined Core-Shell Structures based on Gold Nanoparticles and Metal-Organic Networks

Revital Kaminker,[†] Michal Lahav,[†] Marc Altman,[†] Guennadi Evmenenko,[§]
Pulad Dutta,[§] Antonino Gulino[‡], and Milko E. van der Boom^{*†}

[†]Departments of Organic Chemistry, Weizmann Institute of Science, Rehovot 76100, Israel.

[§] Department of Physics and Astronomy, Northwestern University, Evanston, IL 60208-3112, USA.

[‡]Dipartimento di Scienze Chimiche, Università di Catania, Catania 95125, Italy.

E-mail: milko.vanderboom@weizmann.ac.il

Materials and Methods

Chemicals were purchased from Sigma-Aldrich and Acros Organics. Solvents were reagent grade (AR) from either Bio-Lab (Jerusalem) or Frutarom (Haifa). Pentane and toluene were dried using an M. Braun solvent purification system and degassed before being introduced into an M. Braun glovebox. Acetonitrile (anhydrous, 99.98%) was purchased from Aldrich. Chromophore **1**,¹ PdCl₂(PhCN)₂,² citrate-stabilized AuNPs,^{3, 4} and the pyridyl-terminated monolayer (Scheme S1)⁵ were prepared as reported. Sodium tetrachloroaurate(III) dihydrate was purchased from ABCR GmbH & Co. All glassware used for AuNP formation were cleaned with aqua regia (3:1 v/v, HCl/HNO₃), washed with deionized (DI) water, and with triple-distilled water (TDW). *Caution: aqua regia solutions are extremely corrosive and may result in explosion or skin burns if not handled with extreme caution and appropriate personal protection.* The formation of citrate-stabilized AuNPs was confirmed by TEM, showing an average nanoparticle diameter of 11.8 ± 1.3 nm and by UV/vis spectroscopy, which showed a band at λ_{max} = 518 nm in TDW. Single-crystal silicon (100) substrates were purchased from Wafernet (San Jose, CA) and were cleaned by sonication in hexane followed by acetone, then ethanol, and finally dried under an N₂ stream. Subsequently, they were cleaned for 20 min with UV and ozone in a UVOCS cleaning system (Montgomery, PA). Quartz substrates (Chemglass, Inc.) were cleaned by immersion in a “piranha” solution (7:3 (v/v) H₂SO₄/30% H₂O₂) for 1 h. (*Caution: piranha solution is an extremely dangerous oxidizing agent and should be handled with care using appropriate personal protection.*) Subsequently, the substrates were rinsed with deionized (DI) water followed by the RCA (Radio Corporation of America)⁶ cleaning protocol: 1:5:1 (v/v) NH₄OH/H₂O/30% H₂O₂ at room temperature for 45 min. The substrates were washed with ample amounts of DI water and thereafter were dried under an N₂ stream. Finally, all substrates were then dried in an oven for 2 h at 130°C.

Transmission electron microscopy (TEM). Samples were prepared by depositing a drop of the AuNP-containing solutions on glow-discharged 400-mesh carbon-coated grids and blotting after 60 s. The samples were analyzed with a Philips (FEI-Company, Holland) CM-120 TEM operating at 120 kV. The images were recorded with a Gatan (Gatan USA) Ultrascan 1000 2k × 2k CCD camera.

UV/vis spectra were recorded on a Cary 100 spectrophotometer in double beam transmission mode.

Spectroscopic ellipsometry was recorded on an M 2000 V (J. A. Wollam Co., Inc.) variable-angle spectroscopic ellipsometry (VASE32) at the range of 50°-80° (with 5°

intervals) over wavelengths of 399-1000 nm. The coupled oscillator Lorentz model was used to analyze the data.

High-resolution scanning electron microscope (HRSEM) imaging was carried out with a LEO-Supra 55 VP HRSEM with a 5 kV e beam.

Angle-resolved X-ray photoelectron spectra (AR-XPS) Measurements were performed on silicon and quartz substrates at five different take-off angles, relative to the surface plane (5°, 15°, 30°, 45°, 80°) with a PHI 5600 Multi Technique System (base pressure of the main chamber 2×10^{-10} Torr). The acceptance angle of the analyzer and the precision of the sample holder concerning the takeoff angle are $\pm 3^\circ$ and $\pm 1^\circ$, respectively. The silicon slides were radiated using a monochromator that allowed a resolution of 0.28 eV. Samples were mounted on Mo stubs. Spectra were excited with Al K α radiation. The structure due to satellite radiation has been subtracted from the spectra before the data processing. High-resolution spectra of C(1s), O(1s), Si(2p), N(1s), Pd(3d), and Cl(2p) were collected with 5.85 eV pass energy and a resolution of 0.28 eV and 0.45 eV for silicon and quartz, respectively. The XPS peak intensities were obtained after Shirley background removal and Gaussian line shapes were used for the curve fitting in the data analysis. The C(1s) line at 285.0 eV was used for calibration. A film thickness of 90-100 Å can be probed that corresponds to three times the inelastic mean free path of photoelectrons.

Synchrotron X-ray Reflectivity (XRR) studies were performed at beamline X18A of the National Synchrotron Light Source (NSLS; Brookhaven National Laboratory, USA), using a Huber four-circle diffractometer in the specular reflection mode (i.e., the incident angle is equal to the exit angle θ). The reflected intensity was measured as a function of the scattering vector component $q_z = (4\pi / \lambda) \sin \theta$, perpendicular to the reflecting surface. X-rays of energy $E = 10$ keV ($\lambda = 1.240$ Å) were used with a beam size of 0.5 mm vertically and 1.0 mm horizontally. The resolution was 3×10^{-3} Å $^{-1}$. The samples were placed under a slight overpressure of helium during the measurements to reduce the background scattering from the ambient gas and radiation damage. The off-specular background was measured and subtracted from the specular counts. Details of the data acquisition and analysis are given elsewhere.⁷⁻⁸ The XRR measurements were performed at 20–25°C. The width of X-ray spot on the sample was 1 mm, and the length of X-ray spot (along X-rays) varies as function of the incident angle. At the beginning of the XRR pattern (at the lowest q) X-rays completely cover the sample's along X-rays (8 mm), at the end ($q_z = 0.7$ Å $^{-1}$) - 7 mm – practically the full length of the sample. The Kiessig regions on the XRR patterns (which is mainly responsible for structural data obtained) lie

up to $q_z = 0.3 \text{ \AA}^{-1}$; fitting was done at q_z up to 0.4 \AA^{-1}), which means that we can consider that the XRR beam covers the sample completely and that the average size for obtaining structural data was 1 mm by 8 mm. The electron density of the AuNPs can be calculated from the chemical composition of the material according to the relationship: $\rho = \sum_i b_i \cdot d \cdot N_A / M = (79 \cdot 19.3 \cdot 6.022) / (197 \cdot 10) = 4.66 \text{ e\AA}^{-3}$. Where b_i is the atomic scattering factor for the i^{th} atom (the summation is carried out over all atoms), N_A is Avogadro's number, M is the molar mass, and d is the physical density of the substance. In our case $\sum_i b_i = 79$, $N_A = 6.022 \cdot 10^{23} \text{ mol}^{-1}$, $M = 197 \text{ g/mol}$, and $d = 19.3 \text{ g/cm}^3$. For the electron density of the MON one can consider the AuNPs surface density coverage of 16%, and the experimental electron density profile (Figure 4B, section ii, 1.084 e\AA^{-3}) and finally to derive it from: $4.66 \cdot 0.16 + X(1-0.16) = 1.084$, which results in $X = 0.30 \text{ e\AA}^{-3}$. The electron density profile shown in Figure 4B was obtained by Parratt fitting using a three-slab model having a uniform electron density in each layer and a Gaussian-type interface. The profile shows: (i) a low-density region close to the substrate corresponding to the pyridyl-terminated monolayer. This monolayer is known to have a thickness of $\sim 2 \text{ nm}$, as shown by XRR and ellipsometry measurements, and DFT calculations,⁵ (ii) a relatively high electron density region in the center of the structure that corresponds to the immobilized AuNPs with a diameter of $\sim 12 \text{ nm}$, and (iii) a tail part that indicated the presence of the MON core-shell with a thickness of 3-5 nm. These regions are indicated by the dotted blue lines in Figure 4B.

Formation of gold nanoparticles (AuNP). Sodium citrate (100 mg, 0.34 mmol) was added in one portion to a refluxing rapidly stirred solution of sodium tetrachloroaurate dehydrate (50 mg, 0.13 mmol) in TDW (250 mL). The mixture was stirred under reflux for 15 min before it was allowed to cool to room temperature. The resulting clear solution changed its color from bright yellow to deep red and was stored in a glass bottle sealed from light under air.

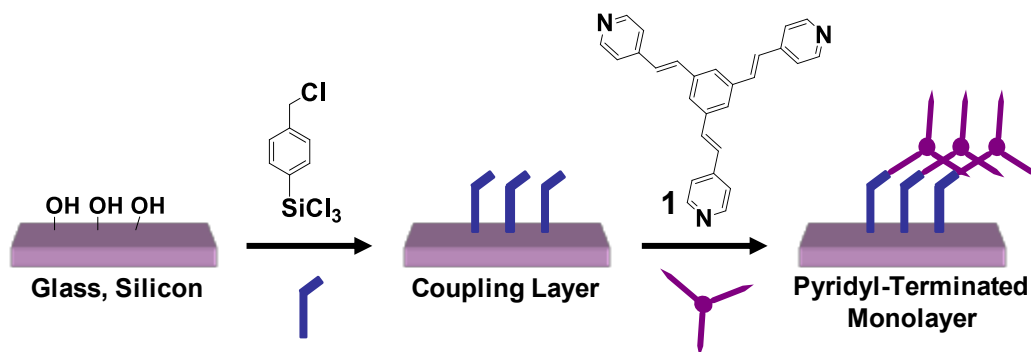
Formation of the Coupling Layer (CL) (Scheme S1).⁵ Freshly cleaned silicon and glass substrates of $0.8 \text{ cm} \times 2.5 \text{ cm}$ were immersed in a solution of trichloro-[4-(chloromethyl)-phenylsilane] ($360 \text{ }\mu\text{L}$, 13 mM) in dry pentane (150 mL) for 1 h at room temperature under N_2 . The substrates were then rinsed in dry pentane (4 \times) and sonicated in pentane, in CH_2Cl_2 , and in *iso*-propanol for 6 min in each solvent. Subsequently, the slides were wiped with Kimwipes wetted with ethanol, sonicated, and dried under a stream of N_2 .

Formation of the pyridyl-terminated monolayer (Scheme S1).⁵ Chromophore **1** (5.8 mg, 0.50 mM) was dissolved in dry toluene (30 mL) by heating to 40°C for 30 min. The

solution was degassed under argon and loaded together with the substrates in a glass pressure tube under N_2 . The sealed tube was heated at $100^\circ C$ for 72 h with the exclusion of light. Subsequently, the slides were sonicated in toluene, CH_2Cl_2 , *iso*-propanol for 6 min in each solvent, cleaned with Kimwipes wetted with ethanol, sonicated again, and finally dried under a stream of N_2 .

Formation of the AuNP-submonolayer. The glass and silicon substrates functionalized with the pyridyl-terminated monolayer (Scheme S1)⁵ were rinsed with TDW (2 \times) and immersed for 1 h in an aqueous AuNP solution (~ 5 mL) at room temperature to provide an AuNP-submonolayer, as judged by AFM and SEM measurements. The samples were then sonicated in TDW for 3 min and rinsed with TDW.

Formation of AuNP-MON with Chromophores 1 and $PdCl_2$ on an AuNP-submonolayer: Substrates functionalized with the AuNP-submonolayer (Scheme 1) were rinsed in THF, immersed in a THF (15 mL) solution of chromophore **1** (5.8 mg, 1.0 mM) for 15 min, sonicated in THF for 3 min and washed again with THF. Subsequently, the samples were immersed in a THF solution (15 mL) of $PdCl_2(PhCN)_2$ (5.8 mg, 1.0 mM) for 15 min, sonicated in THF for 3 min, and then washed with THF. This two-step iterative procedure was carried out 8 times. The formation of the MON was confirmed by UV/Vis and ellipsometric measurements. After each deposition step, the slides were immersed in ethanol and then dried under a stream of N_2 prior to UV/Vis and ellipsometric measurements. A reference experiment was performed in parallel using identical reaction conditions without an AuNP layer. This MON was grown directly on the pyridyl-terminated monolayer.⁵



Scheme S1. Schematic illustration for the assembly of the pyridyl-terminated monolayer with chromophore **1**.⁵ The first step is the functionalization of glass and silicon substrates with trichloro(4-(chloromethyl)phenyl)silane.⁵ The second step represents the covalent attachment of chromophore **1** to the surface.

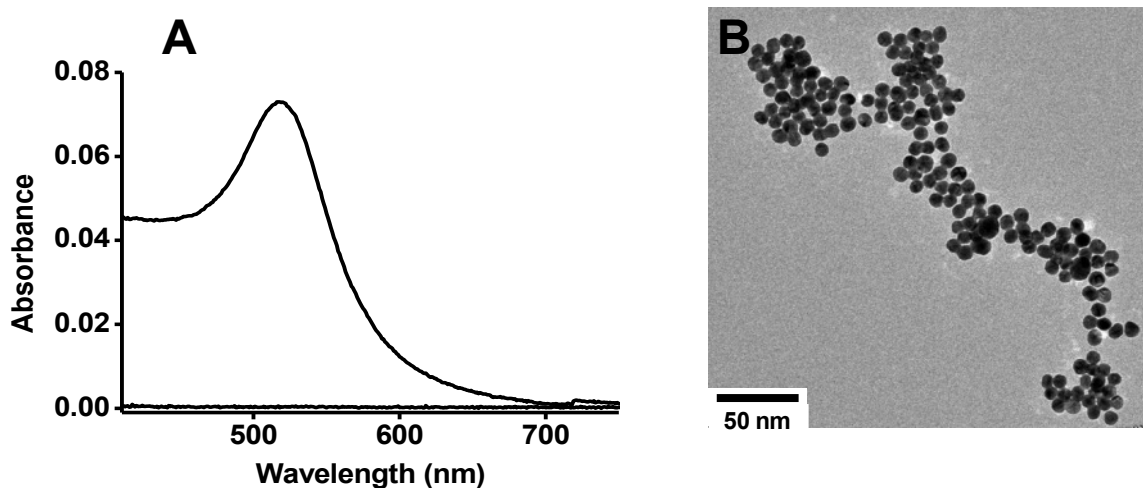


Figure S1. (A) UV/Vis absorption spectrum of the aqueous solution with citrate capped-AuNPs. The baseline was recorded in TDW. (B) Representative TEM image of the AuNPs having an average diameter of 11.8 ± 1.3 nm.

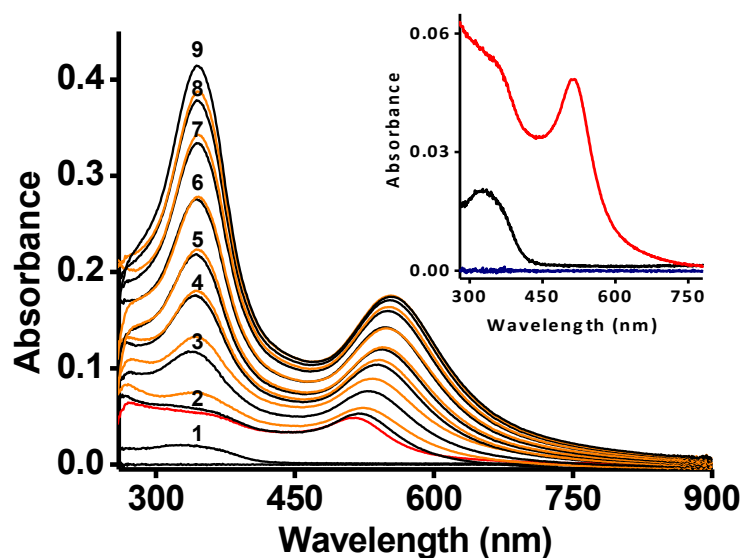


Figure S2. Optical (UV/vis) absorption spectra showing the stepwise formation of **AuNP-MON** on a glass substrate. The first absorption spectrum (1) corresponds to the pyridyl-terminated monolayer. The red spectrum corresponds to the AuNP sub-monolayer. Spectra 2-9 (black) were recorded after each chromophore deposition step, the spectra recorded after the palladium(II) deposition steps are shown in orange. Inset: UV/vis absorption spectra of the AuNP sub-monolayer (red) on a pyridyl-terminated monolayer (black). The baseline (blue) is recorded using a glass substrate.

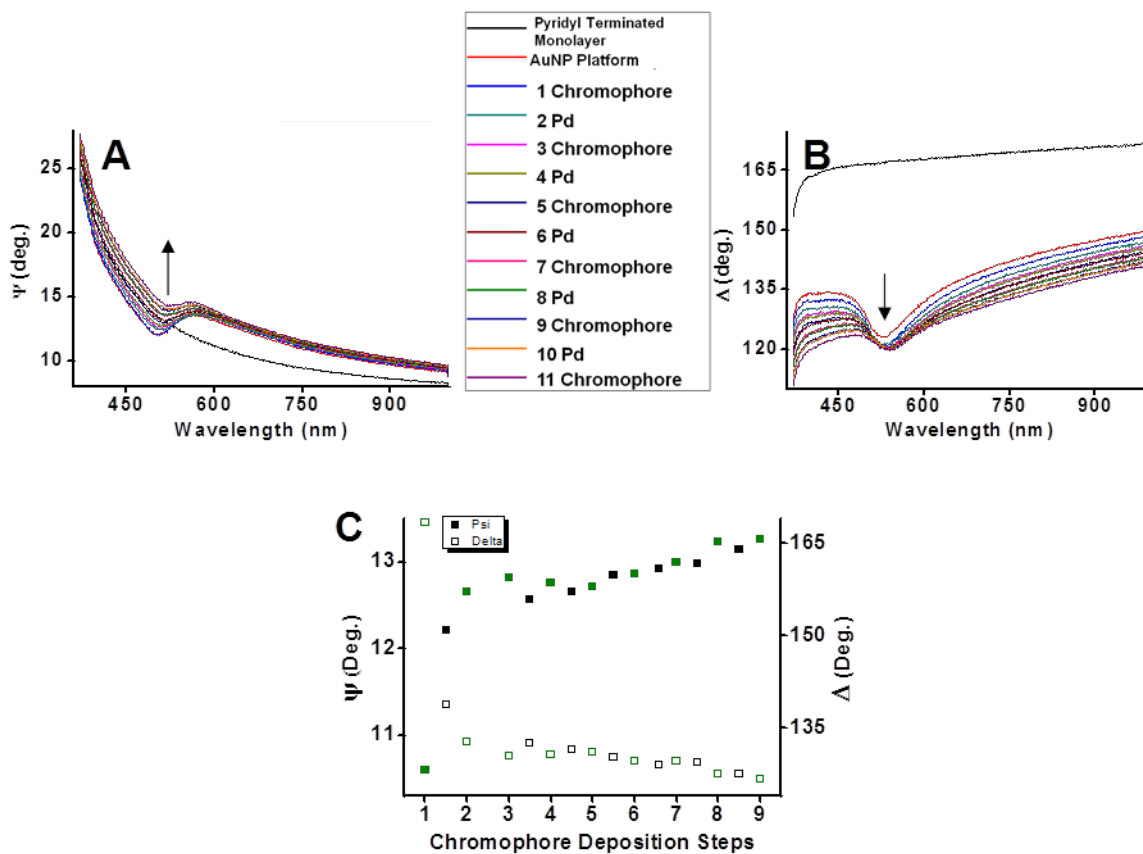


Figure S3. (A) Ψ and (B) Δ , spectroscopic ellipsometry at 70° of **AuNP-MON** on a silicon substrate. Colors: black – pyridyl-terminated monolayer , red – AuNP-submonolayer. (C) Ellipsometry measurements at 70° for Ψ (■) and Δ (□) vs. the number of chromophore and palladium (II) layers in **AuNP-MON**. The green and black data points correspond to the number of chromophore (1) and palladium (II) deposition steps, respectively. Blue data points correspond to the pyridyl-terminated monolayer for Ψ (■) and Δ (□). Phase values were extracted from measurements performed at 70°C at 632.8 nm.

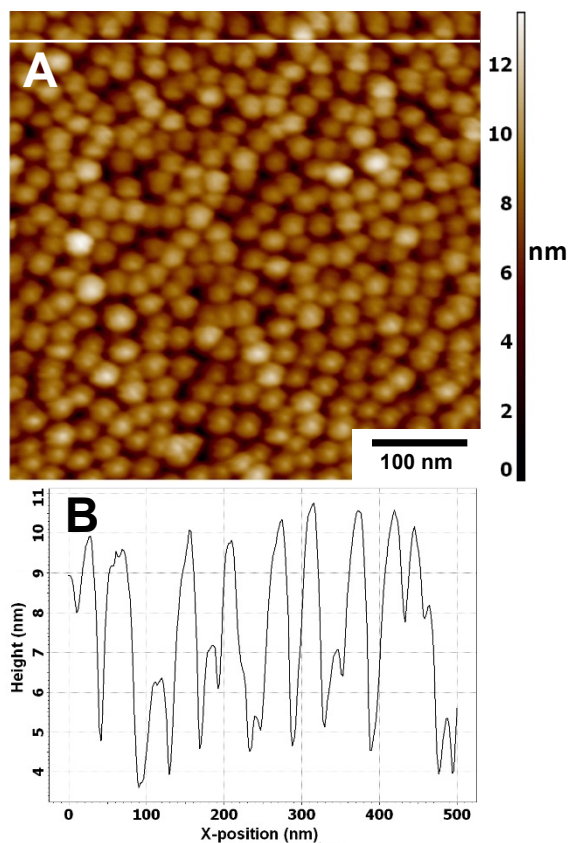


Figure S4. AuNP-submonolayer on silicon substrates: (A) AFM image with a scanning area of 500 nm × 500 nm. (B) Height cross section graph. The location of the cross section is indicated by the white line in image A. The AFM image and the cross-section do not reflect the diameter of the AuNPs because of the limitations imposed by the tip.

5°	15°	30°	45°	80°
0.52	0.55	0.53	0.52	0.53

Table S1. Angle-Resolved XPS measurements. Elemental Pd/N ratios at various take-off angles for **AuNP-MON** on silicon (after 6 chromophore deposition steps).

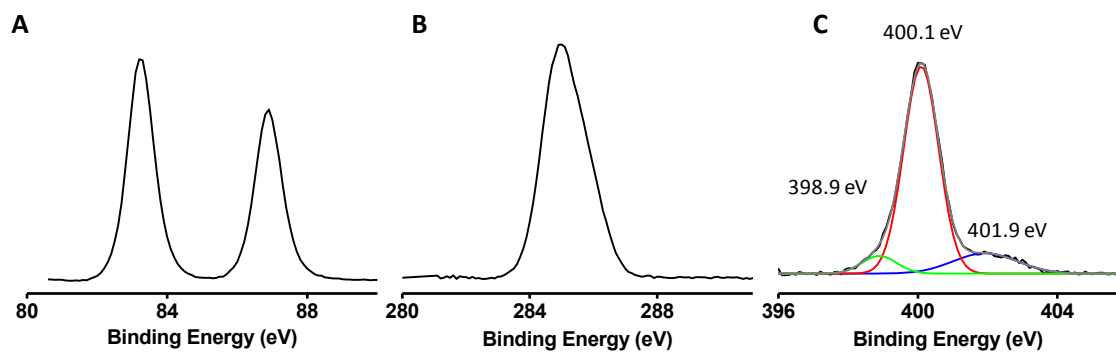


Figure S5. Angle resolved X-ray photoelectron spectroscopy (AR-XPS) spectra for **AuNP-MON** after six chromophore depositions on silicon in the (A) Au 4f (B) C 1s and (C) N 1s binding energy regions. The N 1s region was deconvoluted to resolve the three types of nitrogens. The black trace is the raw data and the grey trace is the fitted cumulative spectrum. The N 1s spectrum shows a main peak at 400.1 eV for N and N-Pd (red), a smaller peak at 401.9 eV for pyridinium N⁺ (blue) and a low binding energy asymmetry at 398.9 eV for N-Au (green).

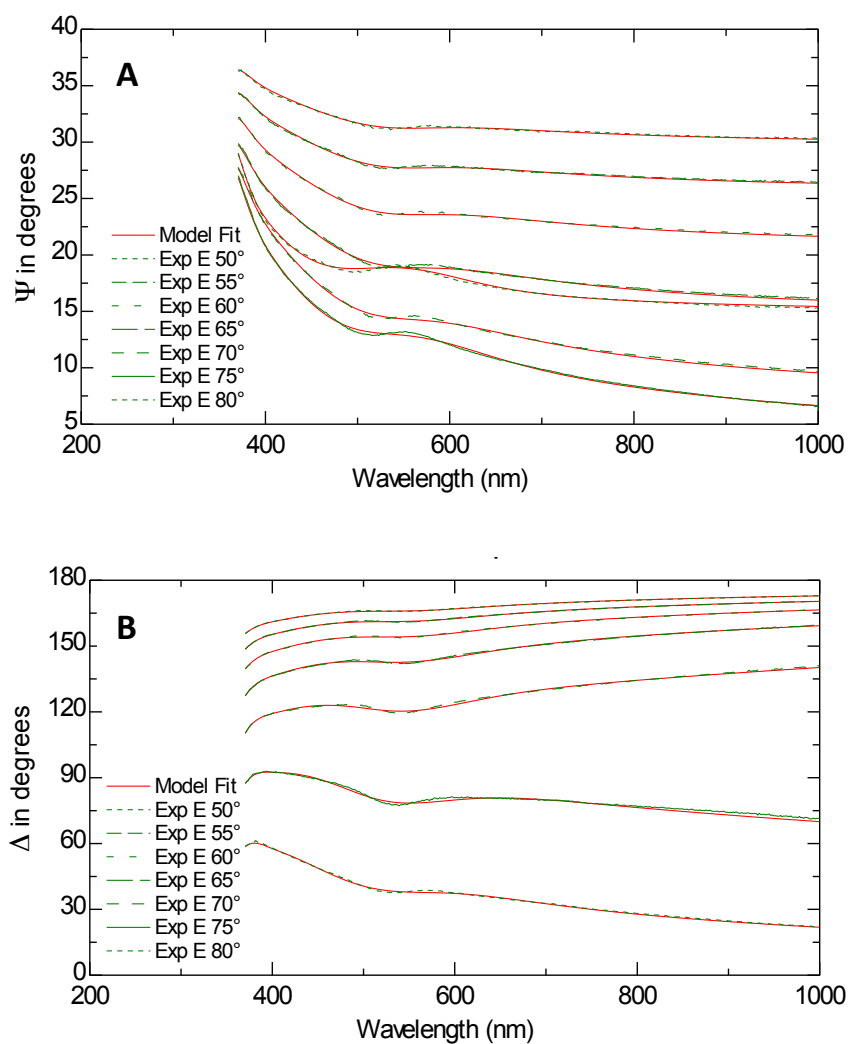


Figure S6. Spectroscopic ellipsometry data A) Ψ and B) Δ for a MON after 6 chromophore deposition steps deposited on a silicon substrate functionalized with a pyridyl-terminated monolayer (Scheme 1). The angle of incidence varies between 50° and 80°. Both experimental (green) and modeled (red) data according to a coupled oscillator Lorentz model⁹⁻¹² are shown.

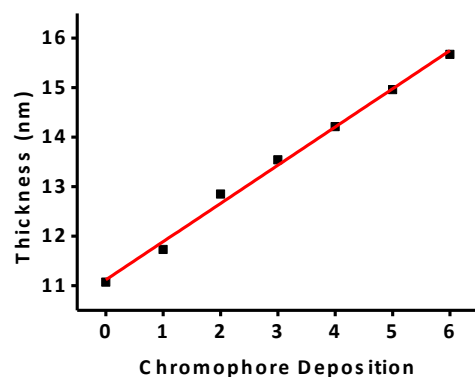


Figure S7. The **AuNP-MON** thickness (ellipsometry) versus the number of chromophore deposition steps. The red line is a linear fit with $R^2 = 0.99$. Point 0 is the AuNP sub-monolayer. These data were derived from ellipsometric measurements on a silicon substrate in which the angle of incidence varied between 50° and 80° .

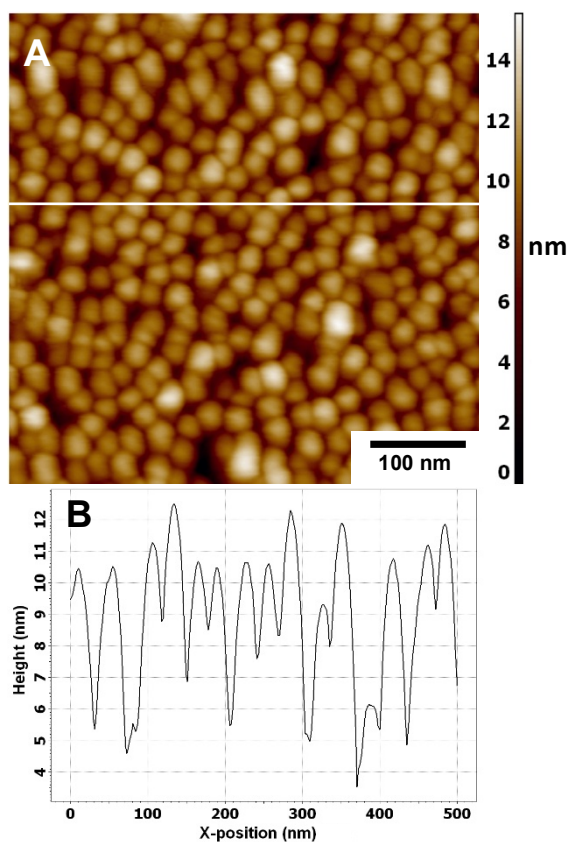


Figure S8. (A) AFM image for **AuNP-MON** after six chromophore depositions on silicon with a scanning area of $500 \text{ nm} \times 500$. (B) Height cross section graph. The location of the cross section is indicated by the white line in image A. The AFM image and the cross-section do not reflect the diameter of the AuNPs because of the limitations imposed by the tip.

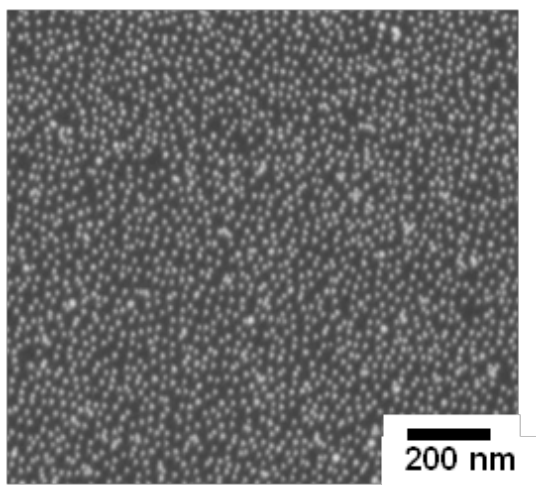


Figure S9. SEM image for **AuNP-MON** after six chromophore deposition steps on silicon with a scanning area of $1.2 \mu\text{m} \times 1.2 \mu\text{m}$. The particle diameter is $\sim 10 \text{ nm}$, and the surface coverage is $\sim 17 \%$.

Notes and References

We have shown previously that various nickel, palladium, and platinum salts and even bimetallic complexes can be used for the formation of coordination-based thin films.¹³ Recently, Gupta and Shalley have demonstrated the use of additional metal salts to growth coordination-based structures.¹⁴

Transmission electron microscope (TEM) measurements show an average AuNP diameter of $\sim 12 \text{ nm}$. Therefore, the projection of a surface-confined AuNP is $\pi r^2 = 3.14 \times 6^2 = 113 \text{ nm}^2$. The scanning electron microscope (SEM) measurements show ~ 350 AuNPs on a surface area of $500 \text{ nm} \times 500 \text{ nm}$ (Figure 1B). The AuNP surface coverage is $350 \times 113 \text{ nm}^2 = 39550 \text{ nm}^2 \rightarrow 39550 \text{ nm}^2 / (500 \text{ nm} \times 500 \text{ nm}) \times 100\% = 16\%$.

- 1 A. J. Amoroso, A. M. W. C. Thompson, J. P. Maher, J. A. McCleverty, M. D. Ward, *Inorg. Chem.*, 1995, **34**, 4828.
- 2 G. K. Anderson, M. Lin, *Inorg. Synth.*, 1990, **28**, 60.
- 3 J. Turkevich, P. C. Stevenson, J. Hillier, *Farad. Discuss.*, 1951, **11**, 55.
- 4 J. Kimling, M. Maier, B. Okenve, V. Kotaidis, H. Ballot, A. Plech, *J. Phys. Chem. B*, 2006, **110**, 15700.
- 5 R. Kaminker, L. Motiej, A. Gulino, I. Fragalà, L. J. W. Shimon, G. Evmenenko, P. Dutta, M. A. Iron, M. E. van der Boom, *J. Am. Chem. Soc.*, 2010, **132**, 14554.
- 6 M. Itano, F. Kern, Jr., M. Miyashita, T. Ohmi, *IEEE Trans. Semicond. Manuf.*, 1993, **6**, 258.
- 7 G. Evmenenko, M. E. van der Boom, J. Kmetko, S. W. Dugan, T. J. Marks, P. Dutta, *J. Chem. Phys.*, 2001, **115**, 6722; G. Evmenenko, B. Stripe, P. Dutta, *J. Colloid Interface Sci.*, 2011, **360**, 793.
- 8 L. G. Parratt, *Phys. Rev.*, 1954, **95**, 359.
- 9 M. Brust, D. Bethell, C. J. Kiely, D. J. Schiffrin, *Langmuir*, 1998, **14**, 5425.

- 10 H.-L. Chen, H.-C. Cheng, T.-S. Ko, S.-Y. Chuang, T.-C. Chu, *Jpn. J. Appl. Phys., Part 1*, 2006, **45**, 6984.
- 11 S. Kubo, A. Diaz, Y. Tang, T. S. Mayer, I. C. Khoo, T. E. Mallouk, *Nano Lett.*, 2007, **7**, 3418.
- 12 H. L. Zhang, S. D. Evans, J. R. Henderson, *Adv. Mater.*, 2003, **15**, 531
13. L. Motiei, M. Feller, G. Evmenenko, P. Dutta, M. E. van der Boom, *Chem Sci.*, 2012, **3**, 66-71; M. Altman, O. V. Zenkina, T. Ichiki, M. A. Iron, G. Evmenenko, P. Dutta, M. E. van der Boom, *Chem. Mater.*, 2009, **21**, 4676.
14. S. Richter, C. H.-H. Traulsen, T. Heinrich, J. Poppenberg, C. Leppich, M. Holzweber, W. E. S. Unger, C. A. Schalley, *J. Phys. Chem. C*, 2013, **117**, 18980; P. C. Mondal, J. Y. Lakshmanan, H. Hamoudi, M. Zharnikov, T. Gupta, *J. Phys. Chem. C*, 2011, **115**, 16398.